nature climate change

LETTERS

https://doi.org/10.1038/s41558-019-0505-x

Strengthening tropical Pacific zonal sea surface temperature gradient consistent with rising greenhouse gases

Richard Seager*, Mark Cane, Naomi Henderson, Dong-Eun Lee, Ryan Abernathey and Honghai Zhang

As exemplified by El Niño, the tropical Pacific Ocean strongly influences regional climates and their variability worldwide[1-3]. It also regulates the rate of global temperature rise in response to rising GHGs[4]. The tropical Pacific Ocean response to rising GHGs impacts all of the world's population. State-of-the-art climate models predict that rising GHGs reduce the west-to-east warm-to-cool sea surface temperature gradient across the equatorial Pacific[5]. In nature, however, the gradient has strengthened in recent decades as GHG concentrations have risen sharply[5]. This stark discrepancy between models and observations has troubled the climate research community for two decades. Here, by returning to the fundamental dynamics and thermodynamics of the tropical ocean–atmosphere system, and avoiding sources of model bias, we show that a parsimonious formulation of tropical Pacific dynamics yields a response that is consistent with observations and attributable to rising GHGs. We use the same dynamics to show that the erroneous warming in state-of-the-art models is a consequence of the cold bias of their equatorial cold tongues. The failure of state-of-the-art models to capture the correct response introduces critical error into their projections of climate change in the many regions sensitive to tropical Pacific sea surface temperatures.

Over the Pacific, easterly trade winds at the Equator drive water westward, creating high sea level and a deep thermocline (the sharp boundary between the warm upper and cool deep ocean) in the west, and low sea level and a shallow thermocline in the east. Because of the Earth's rotation, the trades drive waters away from the Equator, causing upwelling. Upwelling and a shallow thermocline create the equatorial cold tongue in the east and a sea surface temperature (SST) gradient towards the West Pacific warm pool (WPWP). The strength of the gradient varies over time. During warm, El Niño phases of the El Niño–Southern Oscillation, the SST gradient and easterly winds weaken, and deep convection in the atmosphere moves from the WPWP to the normally cooler central equatorial Pacific (CEP) and eastern equatorial Pacific (EEP). In a coupled atmosphere–ocean process, weakened easterlies reduce upwelling, causing warming, and the weaker SST gradient further weakens the easterlies, causing the Bjerknes feedback[1]. Wind-driven transient adjustment of the thermocline allows oscillation between El Niño and cold (La Niña) events on interannual and longer time scales[6]. Changes in the SST gradient and location of deep convection are communicated by Kelvin and Rossby waves into global atmospheric circulation and climate anomalies[3]. During La Niña events, many tropical land masses are anomalously wet while drought impacts the extratropical Americas and East Africa[2]. El Niño impacts are approximately opposite. On decadal time scales, an overall stronger than normal SST gradient since 1998 has driven dry conditions in western North America[7] and East Africa[8], and temporarily reduced the rate of global warming in the atmosphere by enhancing the rate of ocean heat uptake[4].

The SST gradient probably also responds to external forcing. Over the period of instrumental measurement of SST, amid near-universal warming, the CEP to EEP has either not warmed or cooled[5] (Fig. 1a,b,g). It has been argued that, in response to rising GHGs, upwelling and the shallow thermocline allow some of the added heat to be diverged away from the cold tongue such that it warms less than the WPWP. The Bjerknes feedback amplifies this forced response, creating stronger trades and a stronger zonal SST gradient[9,10]. In contrast, the Climate Model Intercomparison Project (CMIP; most recently Phase 5 (CMIP5)) models tend to simulate broad warming over the past century, with enhanced warming in the cold tongue[5]. This response has been explained in terms of exponential dependence of saturation vapour pressure on temperature, necessitating a larger SST change to balance enhanced downward longwave radiation in the cooler east than warmer west[11], weakening of the Walker Circulation[12], and limitation of SST increase by cloud feedbacks over the West Pacific[13]. In Fig. 1g, the cold tongue trends over the entire period analysed here (1958–2017) from 88 CMIP5 model runs and 35 runs from the National Center for Atmospheric Research (NCAR) Large Ensemble (LENS) are compared with four observational SST products: two show no overlap with the models, while the other two lie in the low side of the model distribution. If the observed lack of cold tongue warming is a result of natural variability, it would be expected that many of these 123 simulations, which sample model natural variability well, would produce it. Furthermore, it would be expected that the difference between modelled and observed cold tongue SST change would depend on the choice of start and end dates of trends. Instead, a decade of 60-year trends shows a consistent and widening observations-model discrepancy (Fig. 1g). One explanation is that state-of-the-art climate models have biases in simulation of the cold tongue, Intertropical Convergence Zone, and thermocline and zonal asymmetries of the tropical Pacific[14] and, hence, how these respond to rising GHGs. This SST trend discrepancy has implications for climate projections worldwide.

Previous studies have used statistical methods to examine discrepancies between CMIP5 and observed tropical Pacific SST trends, over a shorter period more influenced by changes in the phase of natural decadal variability[15]. Here, we examine a longer

Lamont-Doherty Earth Observatory, Columbia University, Palisades, NY, USA. *e-mail: seager@ldeo.columbia.edu

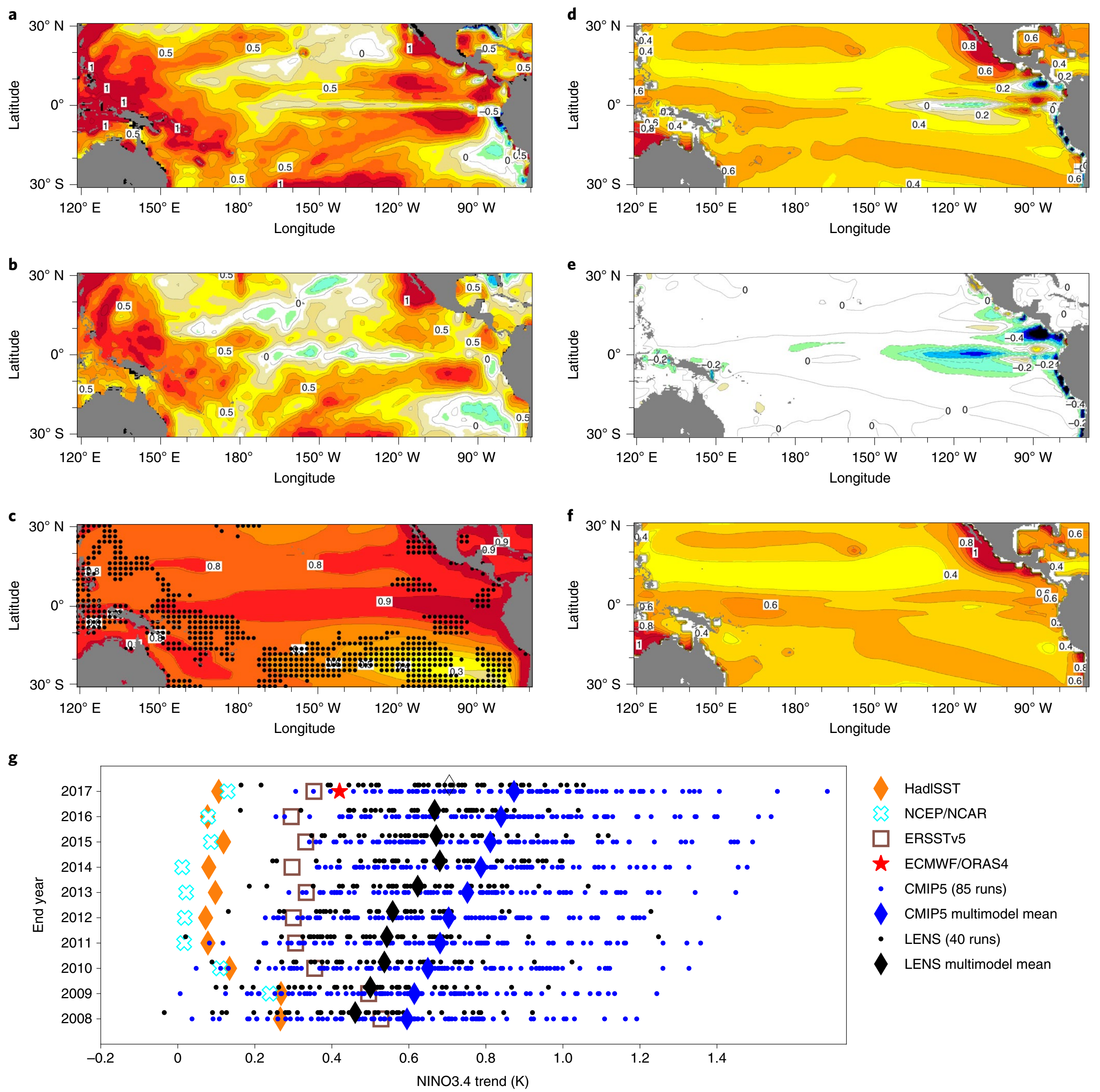

Fig. 1 | SST trends over 1958–2017. a–c, Observed changes in SST (K) according to ECMWF/ORAS4 reanalysis (**a**), HadISST analysis (**b**) and the multimodel mean of 40 historical and RCP8.5 CMIP5 models (**c**), with stippling in **c** showing where the median trend of the CMIP5 models is between the maximum and minimum trends of the four SST analyses. **d–f**, Simulations from the ocean model forced by rising CO_2 and observed winds (**d**), observed winds only, with fixed CO_2 (**e**) and rising CO_2 with fixed winds (**f**). The observed SST trend of no warming in the cold tongue amid widespread warming can be reproduced by the ocean model as a combined thermodynamic and dynamic response to CO_2 and wind stress change. **g**, Distribution of 60-year trends in the NINO3.4 SST index (SST averaged over 5° S–5° N and 170° W–120° W) for end dates from 2008–2017 for 88 individual CMIP5 model runs and 35 NCAR LENS runs, together with observational estimates from ECMWF, HadISST, National Centers for Environmental Prediction (NCEP)/NCAR and ERSSTv5 SST analyses. The observed SST trends ending in the current decade are either colder than, or at the very limit of, the range of trends in individual CMIP5 and LENS model runs.

period and apply fundamental dynamic theory to the problem in three steps. First, with an ocean model with minimal but adequate structure, we show that the observed SST trend is consistent with an ocean response to the observed wind stress change plus increasing CO_2. Second, using a basic atmosphere model, we show that the observed wind stress change is consistent with an atmosphere response to the SST change. Third, we couple the models and show that observed changes in SST and winds are consistent with a coupled response to rising CO_2. To avoid potential sources of bias, and setting them apart from standard CMIP models, our models take

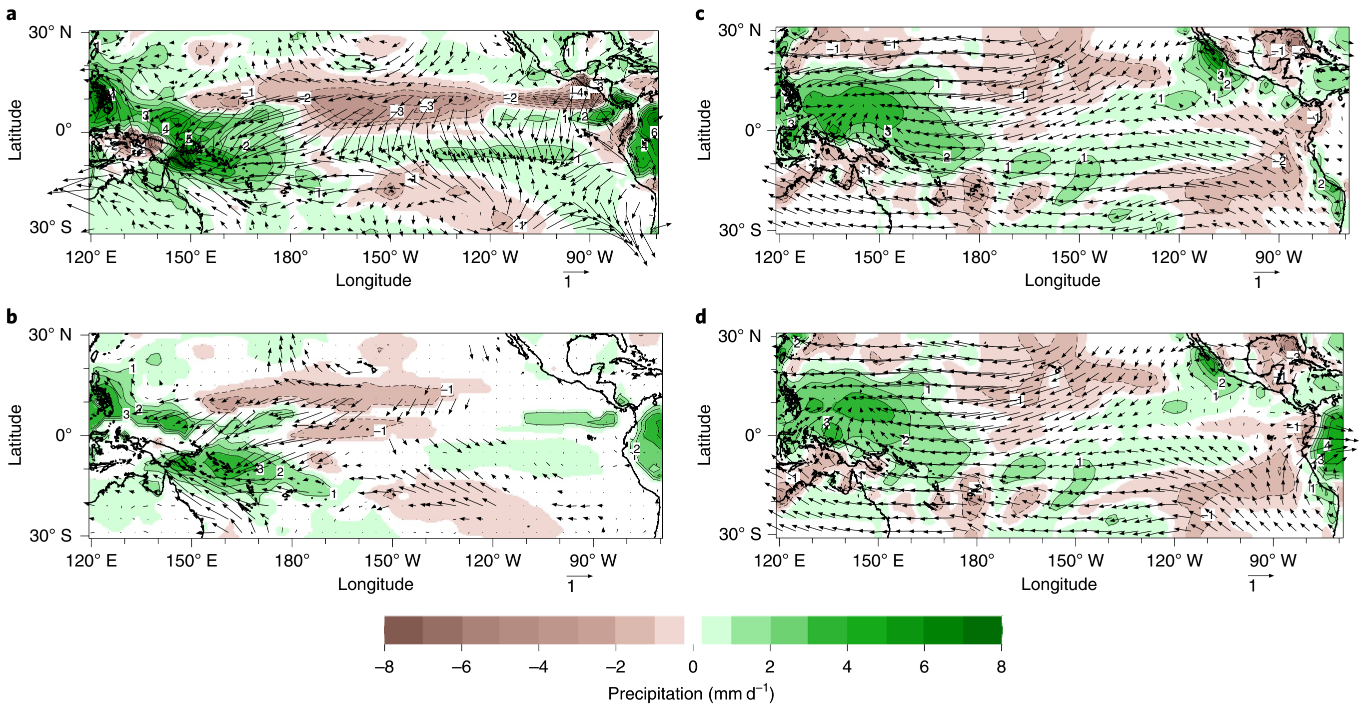

Fig. 2 | Atmosphere trends over 1958–2017. a–d, Trends in surface winds (vectors; the arrow in the bottom right of each panel is a scale bar representing 1 m s^{-1}) and precipitation (colours/contours and numerical labels; see also scale bar), based on ECMWF reanalysis over 1958–2017 (**a**), means from ECMWF, Twentieth Century Reanalysis and Japan Meteorological Agency reanalysis over 1958–2013 (when the Japan Meteorological Agency reanalysis ended), but only where all three agree on the direction of wind trend in the same quadrant and the precipitation trend is of the same sign (**b**), simulations by the atmosphere model forced by the observed ECMWF ORAS4 SST trend only (**c**) and simulations by the atmosphere model forced by trends in ECMWF SST and heating over land (**d**).

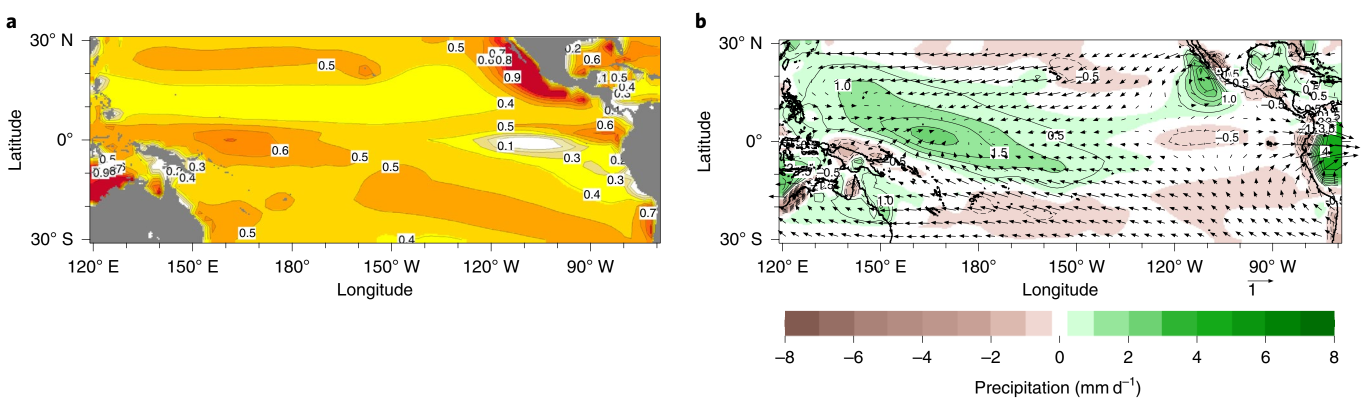

Fig. 3 | Results from the coupled atmosphere and ocean model simulations. a,**b**, SST change (**a**; colours/contours and numerical labels (in K)) and precipitation change (**b**; colours/contours and numerical labels (in mm d^{-1})) for the model forced only by the CO_2 change over 1958–2017 and the precipitation trend over the Amazon. The vectors in **b** represent change in surface wind vectors (scale bar in m s^{-1}).

the climatological mean SST, and vertical structures of the atmosphere and ocean, from data rather than attempting to calculate them. For both fluids, we use linear shallow water equations to describe horizontal motions[16,17] (see Methods). The model atmosphere circulation is driven by radiative relaxation and deep convective heating, calculated using a simple moisture budget. The model SST anomaly is calculated within a uniform-depth mixed layer by balancing SST tendency, horizontal advection, upwelling advection and surface heat fluxes. The ocean sees the atmosphere via surface wind stresses that drive currents and upwelling, and CO_2, surface air temperature and humidity that impact the surface heat flux. The atmosphere sees the ocean via SST, which impacts the surface heat fluxes, air humidity and air temperature, which then influence the precipitation and radiation.

We begin with the ocean response to observed forcing. Figure 1d shows the SST in the ocean model forced by changing European Centre for Medium-Range Weather Forecasts (ECMWF) wind stresses[18–20] and CO_2 over 1958–2017. In both observations and this model (Fig. 1a,d), amid widespread CO_2-induced warming, the central Pacific cold tongue did not warm. When the ocean model is forced by wind stress changes while CO_2 is held constant, the cold tongue cools, indicating a dynamic effect (Fig. 1e).

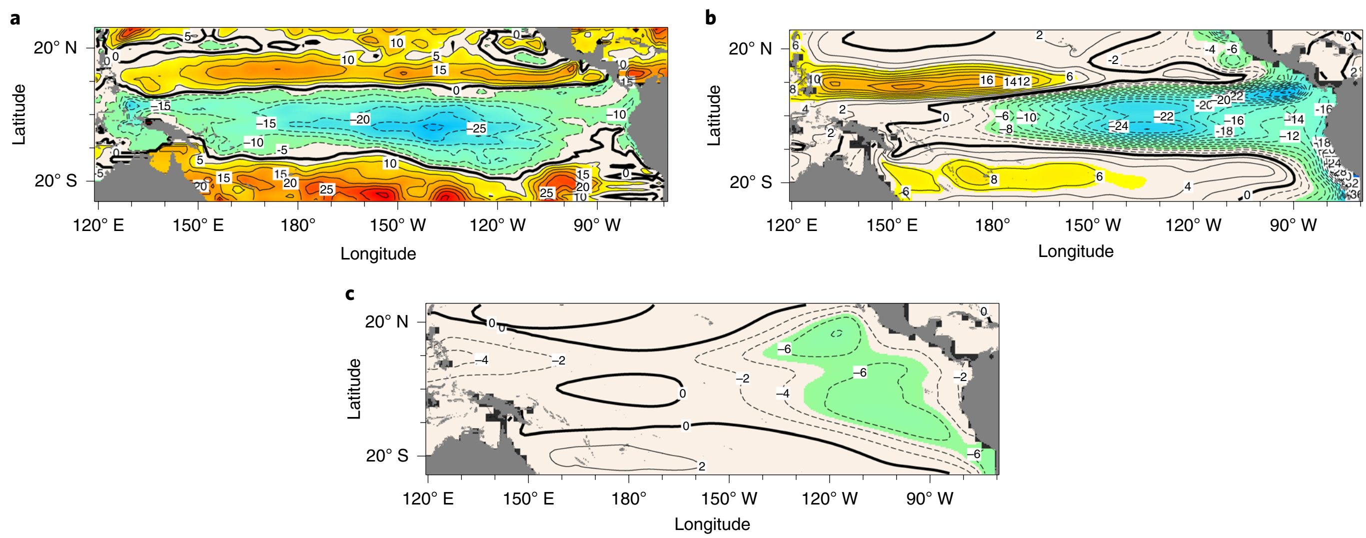

Fig. 4 | Trends in thermocline depth (20 °C isotherm) over 1958–2017. a–c, Results are shown for ORAS4 (**a**), the ocean model forced by the same winds used to force ORAS4 (**b**) and the equilibrium state of our coupled atmosphere–ocean model (**c**). Units for thermocline depth are in m. The coupled model has more wind-forced zonal asymmetry of the equatorial thermocline change than ORAS4, related to differences in equatorial zonal wind stress change. The simulated shoaling in the upwelling region drives the cooling tendency in the cold tongue, and the basin mean component of shoaling is important and driven by off-equatorial trade wind strengthening.

When CO_2 increases but wind stresses are fixed (Fig. 1f), there is warming everywhere, but most where wind speeds are weak (WPWP) and least where wind speeds are strong or there is mean upwelling (regions of weak SST sensitivity to CO_2 forcing; see Methods). The observed tropical Pacific SST trend is largely reproduced according to fundamental ocean physics, as a response to rising CO_2 and changing wind stress, with the ocean dynamic response causing the lack of cold tongue warming.

Turning to trends in the atmosphere, ECMWF reanalysis (Fig. 2a) shows increased precipitation over the WPWP, decreased precipitation over the north central Pacific, and strengthened north and south trades. In Fig. 2b, we plot the average of trends from three reanalyses only where they all agree on the sign of precipitation change and the quadrant containing the direction of wind change. The increased WPWP precipitation and trade wind strengthening are robust across all three products. The atmosphere model forced by the observed change in SST simulates an increase in WPWP precipitation, decreases in precipitation in the east, and overall strengthening of the north and south trades (Fig. 2c), but fails to produce the meridional wind strength (a common failing of such models[21]). Furthermore, reanalyses have westerlies over the CEP to EEP, but the model has easterlies responding to WPWP precipitation. ECMWF reanalyses, and precipitation and surface pressure data, indicate increased Amazon precipitation during this period. We converted the ECMWF tropical land precipitation into atmosphere heating and impose the trend in the SST-forced atmosphere model (Fig. 2d). A westerly equatorial wind response over the EEP to Amazon heating cancels the easterly anomalies, making wind changes more realistic. Overall, strengthening of the trades and the enhanced WPWP precipitation can be reproduced, according to fundamental atmospheric physics, as a response to the SST change over past decades.

Next, we iteratively coupled the atmosphere and ocean models (see Methods) and computed the response to the change in CO_2 alone plus the imposed change in heating over land (Fig. 3). The coupled response has enhanced precipitation over the WPWP, and stronger trade winds. The strengthened winds induce a dynamic cooling tendency in the cold tongue that offsets the CO_2-driven warming. Since the imposed Amazon heating simply induces westerlies over the EEP, it is not responsible for the strengthened trends and resulting enhanced equatorial SST gradient, which instead emerge in response to the imposed CO_2 forcing.

The shoaling thermocline that causes the simulated cold tongue cooling appears in ocean data (Fig. 4a). The shoaling along the equator is well simulated in our ocean model forced by ECMWF winds (Fig. 4b). The coupled model also simulates shoaling (Fig. 4c), but has more east–west tilt due to stronger westward wind stress on the Equator. However, the zonal mean shoaling is caused by off-equatorial trade wind strengthening, consistent with theory[22].

Our coupled model can be used to understand why state-of-the-art models respond to rising GHGs with a greater warming of the cold tongue than elsewhere. To calculate surface heat fluxes and atmospheric moisture convergence, relative humidity is assumed to be spatially uniform in our standard model. If instead we impose the ECMWF distribution, it does not substantially alter the coupled response (Fig. 5a). However, in the CMIP5 multimodel mean relative humidity is too high over the cold tongue (Fig. 5a,b). Also, the CMIP5 climatological wind speed is weaker over the cold tongue than in ECMWF (Fig. 5g,h). When the CMIP5 relative humidity is imposed in our model, the cold tongue warms in response to rising GHGs (Fig. 5b). The response warms by more when the CMIP5 climatological mean wind speed is also imposed in the surface heat flux calculation (Fig. 5c). When additionally the climatological SST in the ocean component is replaced by the CMIP5 climatology, the cold tongue warming in our model closely matches the CMIP5 multimodel mean (Fig. 5d). In this case, the model has no equatorial shoaling of the thermocline (Fig. 5f). We propose that a too-cold cold tongue with warmer water and convergence zones north and south creates, by moisture advection and/or diffusion and wind divergence, a local cold tongue environment of too-high relative humidity and too-low wind speed. These biases create too-high local SST sensitivity to radiative forcing (see Methods). Hence, we argue that cold tongue warming in state-of-the-art models is due to the too-cold cold tongue bias.

Our modelling approach ignores some potentially important large-scale processes, including cloud feedbacks[13], which are hard to identify in the observational record before the satellite era, and the influence on the tropical Pacific of changes in other basins[23].

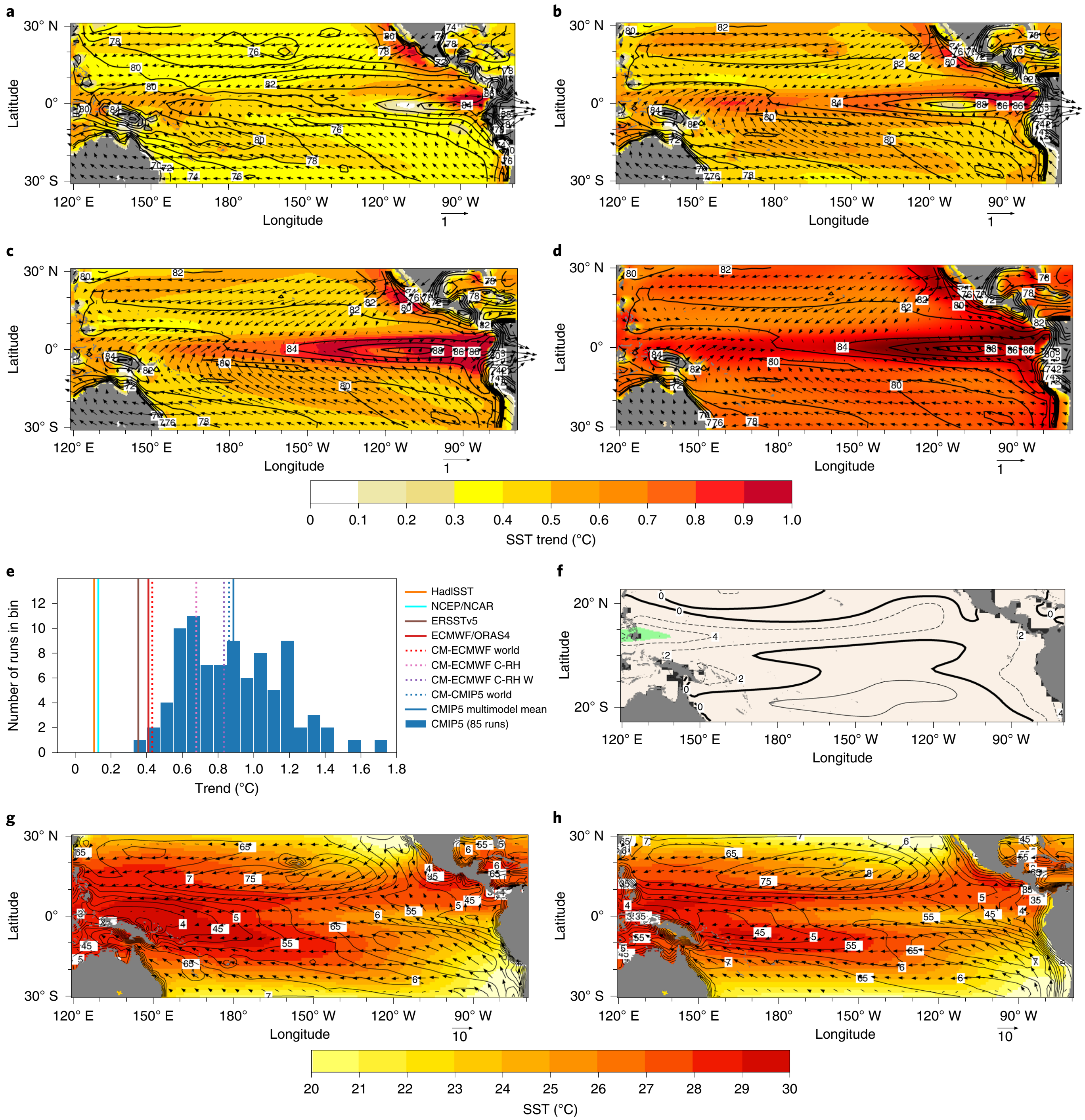

Fig. 5 | Coupled model trends over 1958–2017, and attribution of erroneous trends in CMIP5 models to model bias. a–d, Trends in winds (vectors; scale bar in m s^{-1}) and SST (colours; see scale bar) over 1958–2017 within the coupled model (CM), moving from the observed world to the CMIP5 world. In **a**, the observed spatially varying relative humidity (%, contours) from ECMWF is imposed in the model instead of a uniform value ('CM-ECMWF world' in **e**). In **b**, the CMIP5 multimodel mean spatially varying relative humidity (%, contours in **b–d**) is imposed ('CM-ECMWF C-RH' in **e**). In **c**, the CMIP5 wind speed is also imposed ('CM-ECMWF C-RH W' in **e**). Finally, in **d**, the ocean model is additionally 'q-fluxed' towards the CMIP5 multimodel mean SST climatology ('CM-CMIP5 world' in **e**). **e**, Histogram of trends in the NINO3.4 SST index in 88 individual CMIP5 model runs, together with the trends from HadISST, NCEP/NCAR, ERSSTv5 and ECMWF ORAS4 SST analyses, and our coupled model setups described in **a–d**. The observed SST trends are at the very cold end or beyond the range of trends in individual CMIP5 model runs, but are well matched by our coupled model. **f**, Trends in thermocline depth (m). **g**,**h**, Climatological winds (vectors; scale bar in m s^{-1}), SST (colours; see scale bar) and wind speed (m s^{-1} contours and numerical labels) for ECMWF (**g**) and the CMIP5 multimodel mean (**h**). Incorporating from the CMIP5 multimodel mean the climatological relative humidity, which is biased high over the cold tongue (**a** and **b**), and wind speed, which is biased low over the cold tongue (**g** and **h**), allows our coupled model to match the CMIP5 multimodel mean trend well.

The thermocline structure is fixed in the model, while in nature it could change as the waters that flow into the equatorial thermocline from the subtropics[24] warm. However, this is likely to remain a small influence on the temperature of upwelling water relative to the effect of the wind-driven thermocline shoaling identified here. This is a consequence of the equatorial thermocline being so sharp that even small vertical displacements result in substantial temperature changes. These caveats notwithstanding, the reproduction of key features of observed change by a parsimonious tropical Pacific-centred model suggests that these changes are largely due to local dynamic coupling.

The main features of observed tropical Pacific climate change over past decades are consistent with a response to rising CO_2, according to fundamental atmosphere and ocean physics. The spatial pattern of climatological upwelling and wind speeds means rising CO_2 causes more warming over the western than CEP, driving stronger trade winds that shoal the thermocline, which cools the cold tongue, further strengthening the zonal SST gradient and, hence, the trades. Delayed warming of the thermocline could oppose this positive feedback but, to date, has not cancelled it. This response favours enhanced (diminished) convection over the west (central) equatorial Pacific akin to La Niña events and will drive La Niña-like climate trends worldwide (drying in East Africa, southwest North America and southeast South America, and wetting in Southeast Asia, Northeast Brazil and the Sahel). These tropical Pacific-driven precipitation changes will compete against other sources of variability and radiatively driven change[25,26]. However, the strength of the tropical Pacific influence on global climate implies that past and future trends will diverge from those simulated by coupled climate models that, due to their cold tongue bias, misrepresent the response of the tropical Pacific to rising CO_2. Until state-of-the-art models more faithfully represent the observed tropical Pacific, climate impact assessments should consider the consequences for the global hydroclimate of continuing La Niña-like trends in tropical Pacific SSTs.

Online content

Any methods, additional references, Nature Research reporting summaries, source data, statements of code and data availability and associated accession codes are available at https://doi.org/10.1038/s41558-019-0505-x.

Received: 24 December 2018; Accepted: 10 May 2019;
Published online: 24 June 2019

References

1. Bjerknes, J. Atmospheric teleconnections from the equatorial Pacific. *Mon. Weather Rev.* **97**, 162–172 (1969).
2. Dai, A. & Wigley, T. M. L. Global patterns of ENSO-induced precipitation. *Geophys. Res. Lett.* **27**, 1283–1286 (2000).
3. Trenberth, K. E. et al. Progress during TOGA in understanding and modeling global teleconnections associated with tropical sea surface temperature. *J. Geophys. Res.* **103**, 14291–14324 (1998).
4. Kosaka, Y. & Xie, S.-P. Recent global-warming hiatus tied to equatorial Pacific surface cooling. *Nature* **501**, 403–407 (2013).
5. Coats, S. & Karnauskas, K. B. Are simulated and observed twentieth century tropical Pacific sea surface temperature trends significant relative to internal variability? *Geophys. Res. Lett.* **44**, 9928–9937 (2017).
6. Zebiak, S. E. & Cane, M. A. A model El Niño–Southern Oscillation. *Mon. Weather Rev.* **115**, 2262–2278 (1987).
7. Delworth, T. L., Zeng, F., Rosati, A., Vecchi, G. A. & Wittenberg, A. A link between the hiatus in global warming and North American drought. *J. Clim.* **28**, 3834–3845 (2015).
8. Yang, W., Seager, R., Cane, M. A. & Lyon, B. The East African long rains in observations and models. *J. Clim.* **27**, 7186–7202 (2014).
9. Clement, A. C., Seager, R., Cane, M. A. & Zebiak, S. E. An ocean dynamical thermostat. *J. Clim.* **9**, 2190–2196 (1996).
10. Cane, M. A. et al. Twentieth century sea surface temperature trends. *Science* **275**, 957–960 (1997).
11. Knutson, T. R. & Manabe, S. Time-mean response over the tropical pacific to increased CO_2 in a coupled ocean–atmosphere model. *J. Clim.* **8**, 2181–2199 (1995).
12. Vecchi, G. A. & Soden, B. J. Global warming and the weakening of the tropical circulation. *J. Clim.* **20**, 4316–4340 (2007).
13. Li, G., Xie, S.-P., Du, Y. & Luo, Y. Effects of excessive equatorial cold tongue bias on the projections of tropical Pacific climate change. Part I: the warming pattern in CMIP5 multi-model ensemble. *Clim. Dynam.* **47**, 3817–3831 (2016).
14. Li, G. & Xie, S. P. Tropical biases in CMIP5 multimodel ensemble: the excessive equatorial Pacific cold tongue and double ITCZ problems. *J. Clim.* **27**, 1765–1780 (2014).
15. Luo, J.-J., Wang, G. & Dommenget, D. May common model biases reduce CMIP5's ability to simulate the recent Pacific La Niña-like cooling? *Clim. Dynam.* **50**, 1335–1351 (2018).
16. Gill, A. E. Some simple solutions for heat-induced tropical circulation. *Q. J. R. Meteor. Soc.* **106**, 447–462 (1980).
17. Blumenthal., M. B. & Cane, M. A. Accounting for parameter uncertainties in model verification: an illustration with tropical sea surface temperature. *J. Phys. Oceanogr.* **19**, 815–830 (1989).
18. Uppala, S. M. et al. The ERA-40 re-analysis. *Q. J. R. Meteor. Soc.* **131**, 2961–3012 (2005).
19. Dee, D. P. et al. The ERA-Interim reanalysis: configuration and performance of the data assimilation system. *Q. J. R. Meteor. Soc.* **137**, 553–597 (2011).
20. Balmaseda, M. A., Mogensen, K. & Weaver, A. T. Evaluation of the ECMWF ocean reanalysis system ORAS4. *Q. J. R. Meteor. Soc.* **139**, 1132–1161 (2013).
21. Chiang, J. C. H., Zebiak, S. E. & Cane, M. A. Relative roles of elevated heating and surface temperature gradients in driving anomalous surface winds over tropical oceans. *J. Clim.* **58**, 1371–1394 (2001).
22. Emile-Geay, J. & Cane, M. A. Pacific decadal variability in the view of linear equatorial wave theory. *J. Phys. Oceanogr.* **39**, 203–219 (2009).
23. Hu, S. & Federov, A. V. Cross-equatorial winds control El Niño diversity and change. *Nat. Clim. Change* **8**, 798–802 (2018).
24. Burls, N. J. & Federov, A. V. What controls the mean East–West sea surface temperature gradient in the equatorial Pacific: the role of cloud albedo. *J. Clim.* **27**, 2757–2778 (2014).
25. Seager, R., Naik, N. & Vecchi, G. A. Thermodynamic and dynamic mechanisms for large-scale changes in the hydrological cycle response to global warming. *J. Clim.* **23**, 4651–4668 (2010).
26. Wu, Y. & Polvani, L. M. P. Contrasting short- and long-term projections of the hydrological cycle in the southern extratropics. *J. Clim.* **28**, 5845–5856 (2015).

Acknowledgements

This work was supported by NSF award OCE 1657209 and a grant from World Surf League P.U.R.E. through Columbia University's Center for Climate and Life. We thank R. Miller, B. Fox-Kemper, T. Shepherd, R. Chadwick, J. Smerdon, P. Williams and I. Simpson for useful discussions.

Author contributions

R.S. conceived of the study and directed the research. All authors designed the experiments. R.S. and M.C. designed the atmosphere and ocean thermodynamic models. N.H. and M.C. designed the numerical methods for solution, with assistance from R.S. N.H. wrote the new model codes, implemented the ocean model and conducted the modelling. D.-E.L. and N.H. led the analysis of ocean and atmosphere data. D.-E.L. conducted experiments with the ocean model to interpret the results. R.S. wrote the paper, with all authors contributing advice on content and wording.

Competing interests

The authors declare no competing interests.

Additional information

Reprints and permissions information is available at www.nature.com/reprints.

Correspondence and requests for materials should be addressed to R.S.

Peer review information: *Nature Climate Change* thanks Natalie Burl and the other, anonymous, reviewer(s) for their contribution to the peer review of this work.

Publisher's note: Springer Nature remains neutral with regard to jurisdictional claims in published maps and institutional affiliations.